Enhancing Microcirculation on Multitriggering Manner Facilitates Angiogenesis and Collagen Deposition on Wound Healing by Photoreleased NO from Hemin-Derivatized Colloids

Chia-Hao Su,[§,†] Wei-Peng Li,[§,‡,∥] Ling-Chuan Tsao,[§,‡] Liu-Chun Wang,[‡] Ya-Ping Hsu,[‡,∥] Wen-Jyun Wang,[‡,∥] Min-Chiao Liao,[†] Chin-Lai Lee,[†] and Chen-Sheng Yeh,[,‡,∥,#]*

[†]Institute for Translational Research in Biomedicine, Kaohsiung Chang Gung Memorial Hospital, Kaohsiung, 833, Taiwan.

[‡]Department of Chemistry, National Cheng Kung University, Tainan, 701, Taiwan.

[∥]Center of Applied Nanomedicine, National Cheng Kung University, Tainan, 701, Taiwan.

[#] Department of Medicinal and Applied Chemistry, Kaohsiung Medical University, Kaohsiung, 807, Taiwan.

[§]C.-H. Su, W.-P. Li and L.-C. Tsao contributed equally.

*Correspondence author E-mail: csyeh@mail.ncku.edu.tw

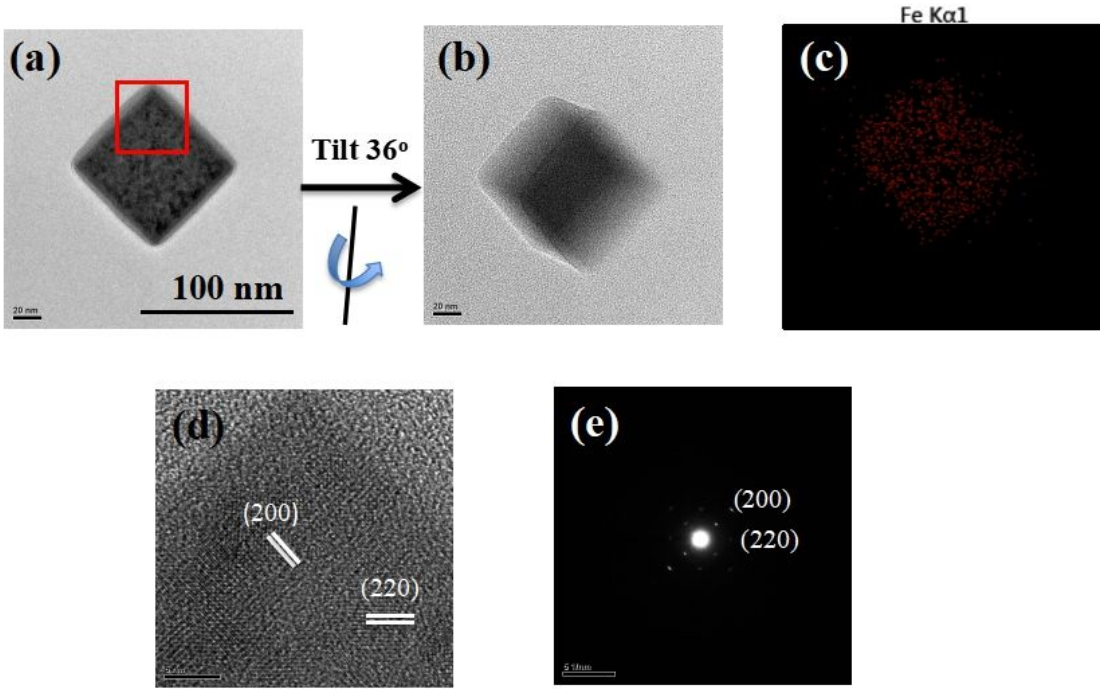

Figure S1. High-resolution transmission electron microscopic (HR-TEM) analysis of PB nanocube. (a) The face-directed image and (b) the vertex-directed image, tilted by 36°. (c) The element mapping analysis showing Fe distribution. (d) High magnification image taken from the red frame shown in (a) giving the crystallographic planes of (200) and (220). (e) The selected area electron diffraction analysis of a PB nanocube showing the single crystalline feature observed from the [001] orientation.

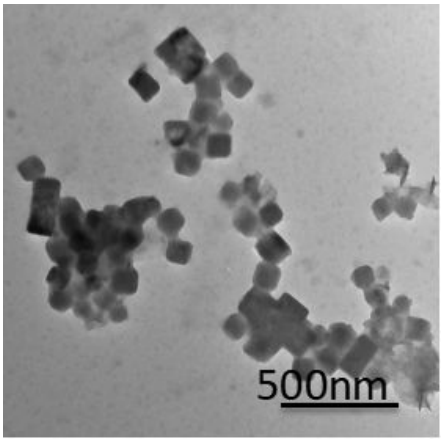

Figure S2. TEM image of the deformed PB-NH_2 nanocubes in aggregation when the reaction time extended to 30 min.

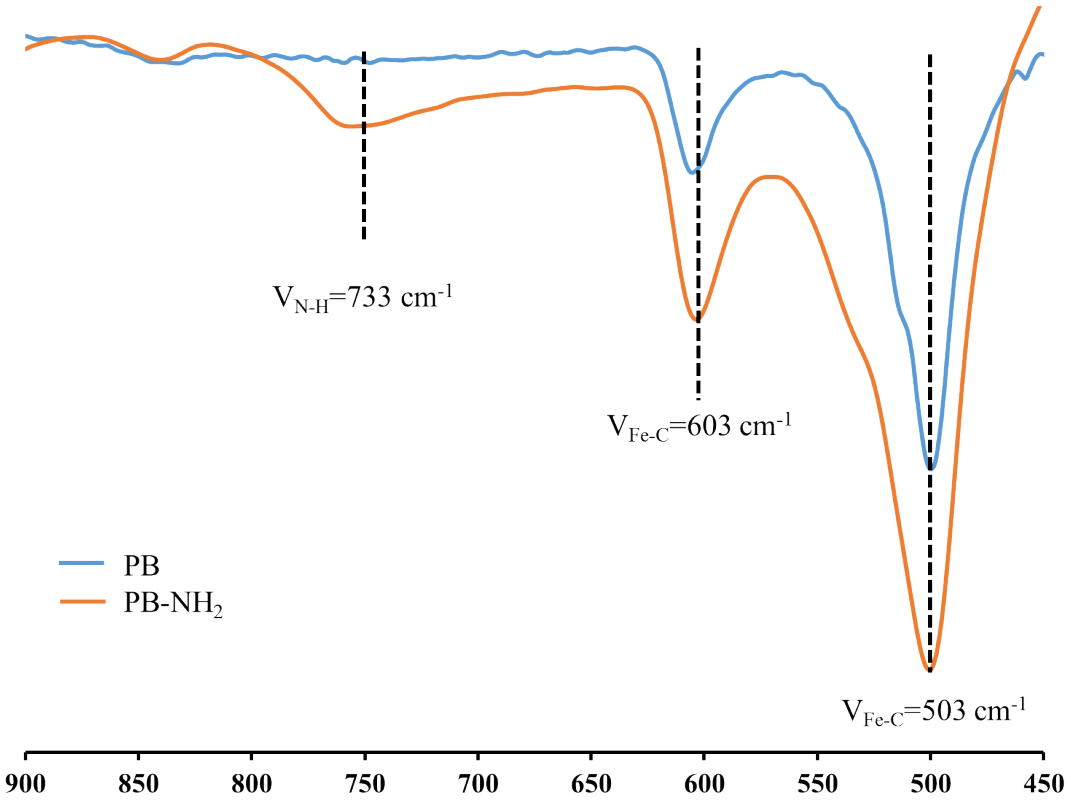

Figure S3. The FTIR spectra of the selected wavelength from 900 cm^{-1} to 450 cm^{-1}in amplification showing the appearance of N-H vibration after PB reduced to PB-NH_2 nanocubes.

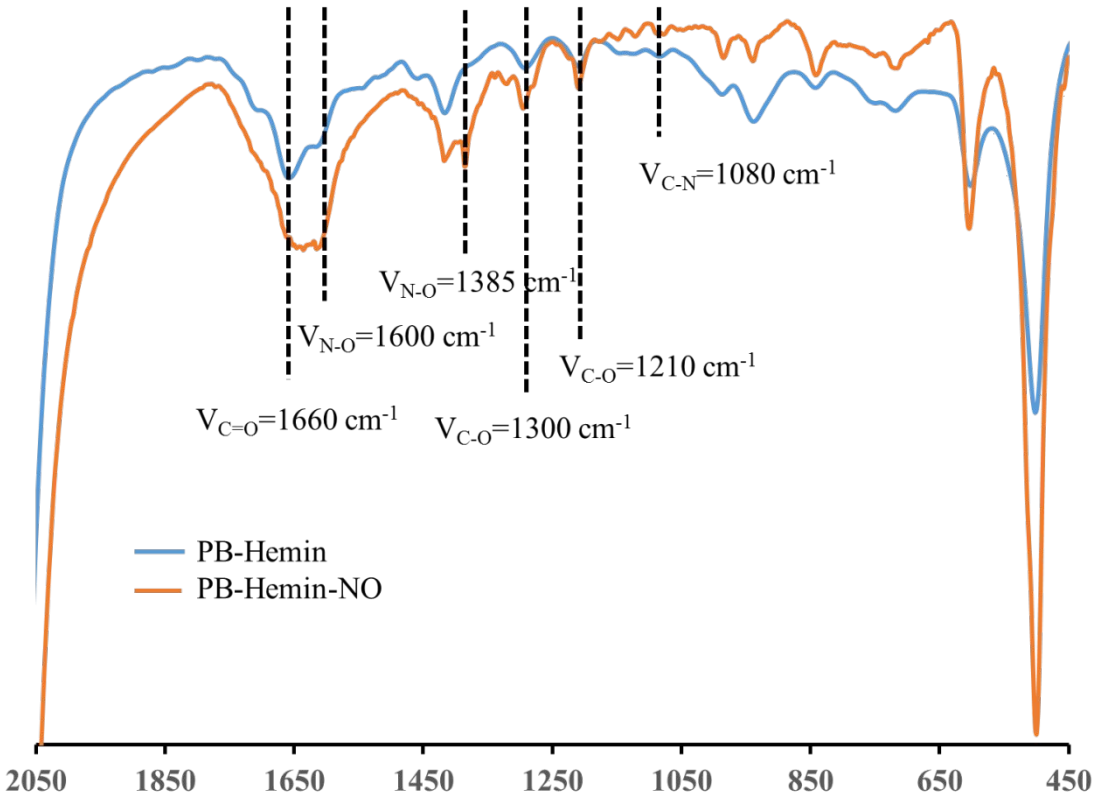

Figure S4. FT-IR analysis of PB-Hemin nanocubes and PB-Hemin-NO (NO-carried PB-Hemin) nanocubes indicating the appearance of the N-O vibrations at 1385 cm^{-1} and an enhanced broad band on 1580-1600 cm^{-1} overlapping with the C=O vibrations.

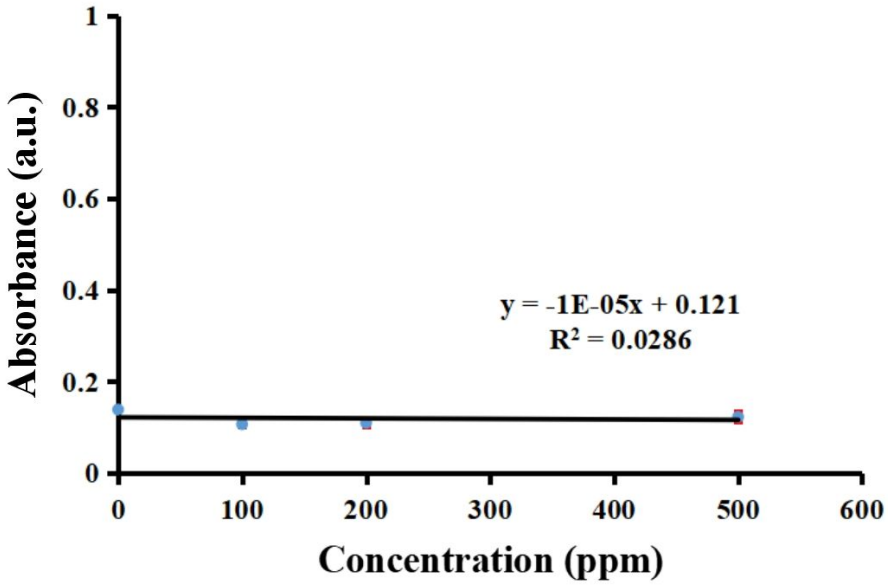

Figure S5. The absorbance of azo compound, a product from the Griess diazotization reaction, was used to determine NO-release amount from NO-loaded PB colloids (without hemin modification) in different dosages (based on iron concentration).

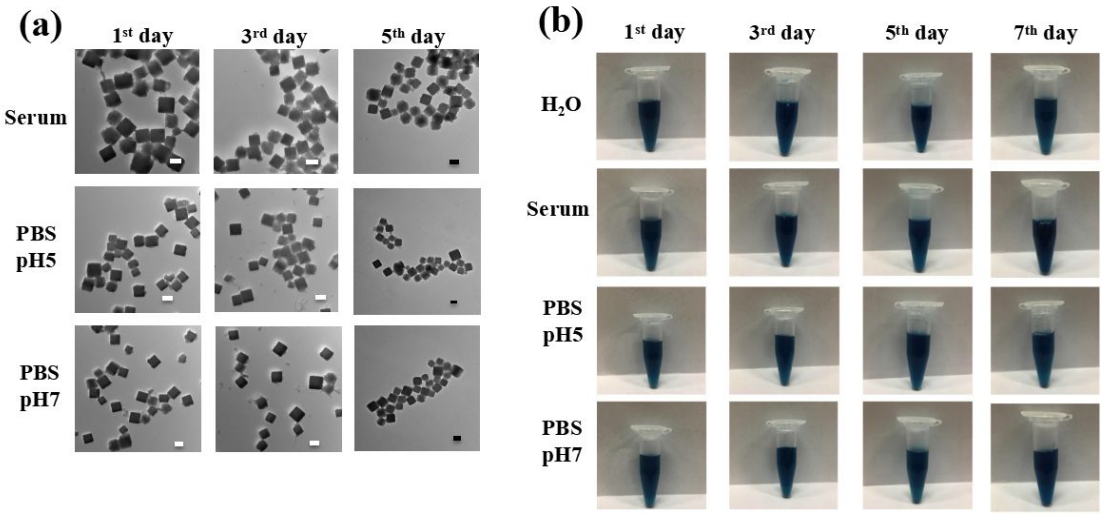

Figure S6. Stability performance of PB-NO nanocubes under different mediums at 37 ^{o}C. The PB-NO nanocubes can be dispersed in H_2O, serum, PBS(pH 5), PBS(pH 7). The TEM images (scale bar = 100 nm) (a) and photographs (b) provide the evidence of the intact structure of PB-NO nanocubes and no occurrence of precipitation for colloidal solutions after a period of 7-day incubation.

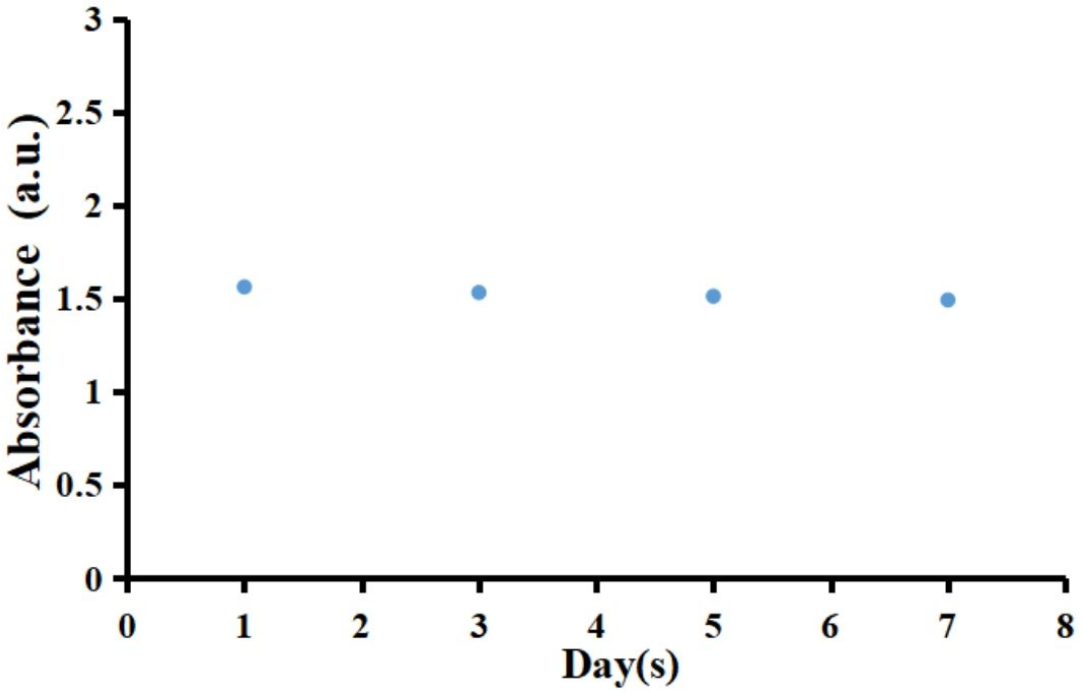

Figure S7. Spectral stability of PB-NO colloids at 37 ^{o}C serum was monitored at 808 nm absorbance through UV-Vis spectra.

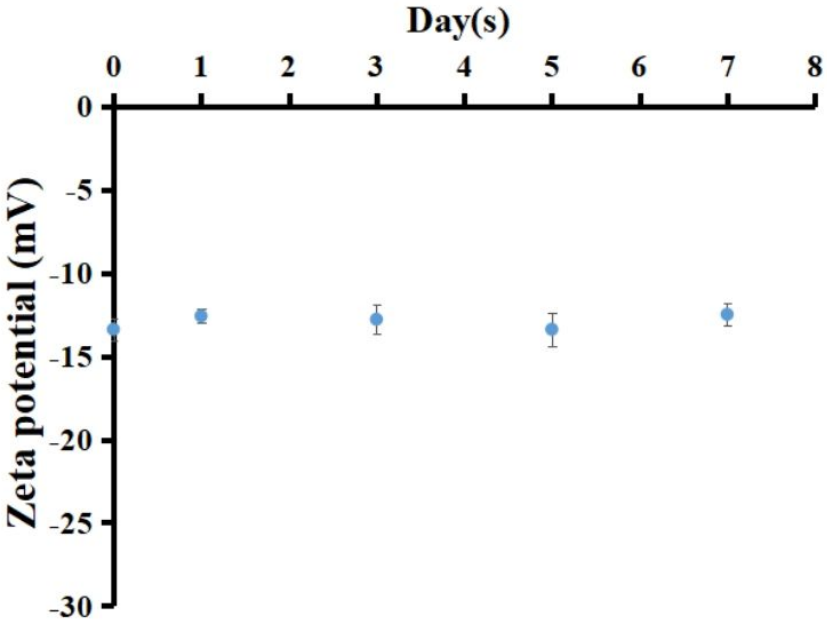

Figure S8. Physical stability through surface charge was conducted when PB-NO colloids were stored in serum at 37 ^{o}C.

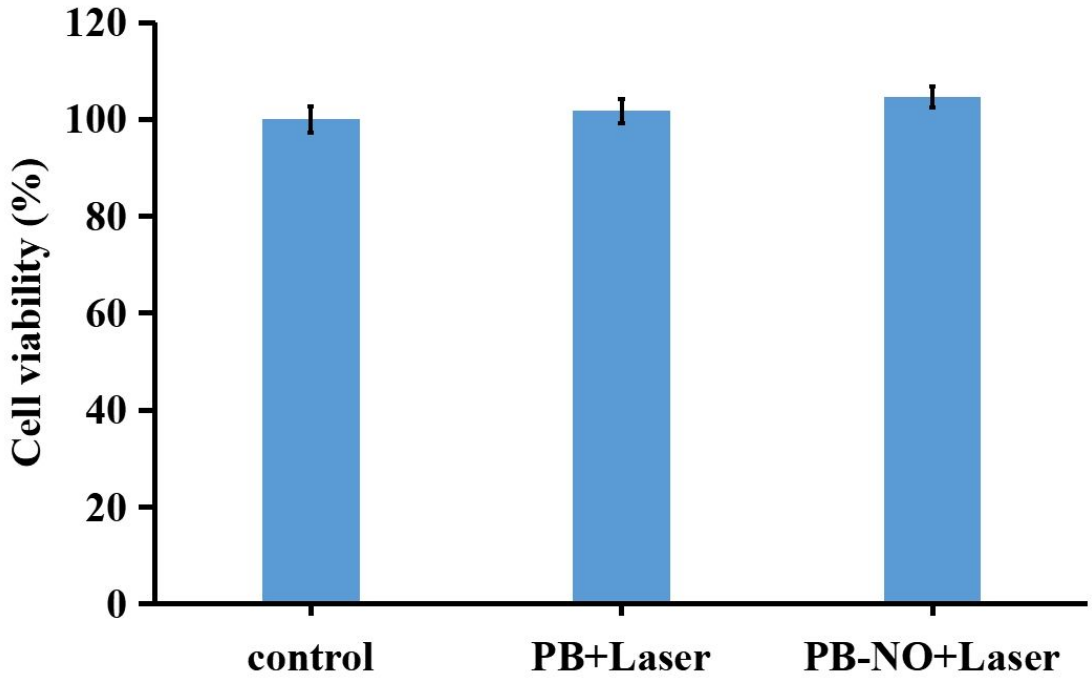

Figure S9. The survival rates of MRC-5 cells when treated with PB and PB-NO colloids (100 ppm) upon 808 nm diode laser exposure at 0.5 W/cm^2 for 10 min. The cell viability was recorded using MTT assays. All of the data were obtained in quadruplicate.

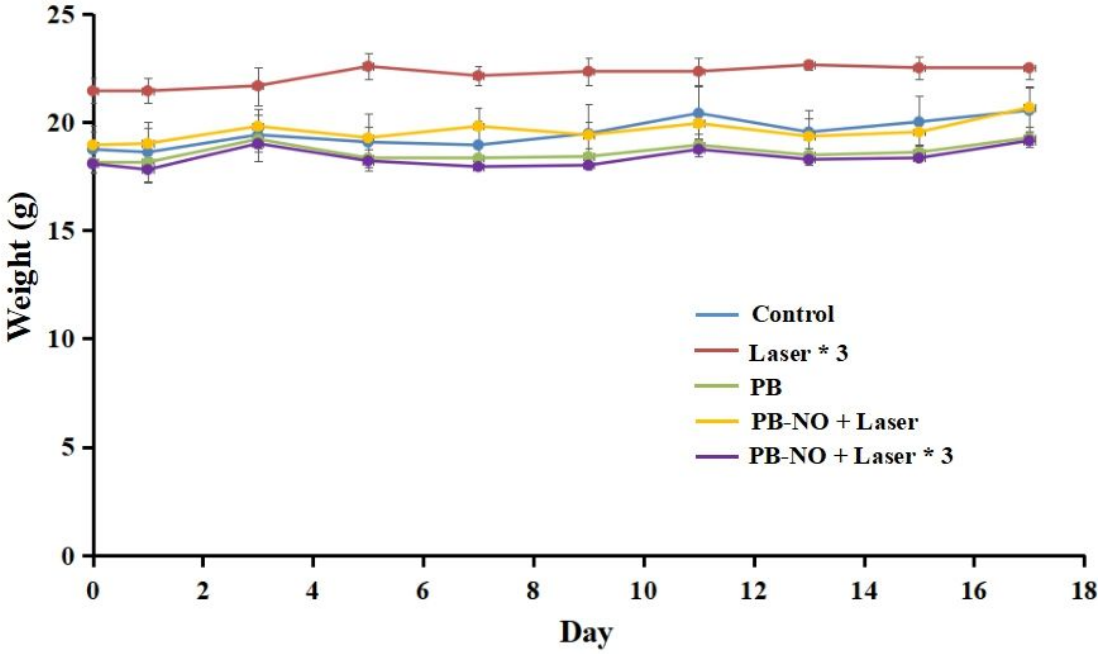

Figure S10. Body weight of mice were observed and showed no unusual change in a period of 20 days following the different treatments of H_2O, H_2O + Laser*3 (referred as Laser*3), PB colloids, PB-NO colloids + Laser, and PB-NO colloids + Laser*3. The groups with laser received 0.5 W/cm^2 exposure for 10 min. The groups showing *3 represent that H_2O + Laser or PB-NO + Laser was respectively repeated in 3 consecutive days on wounds.

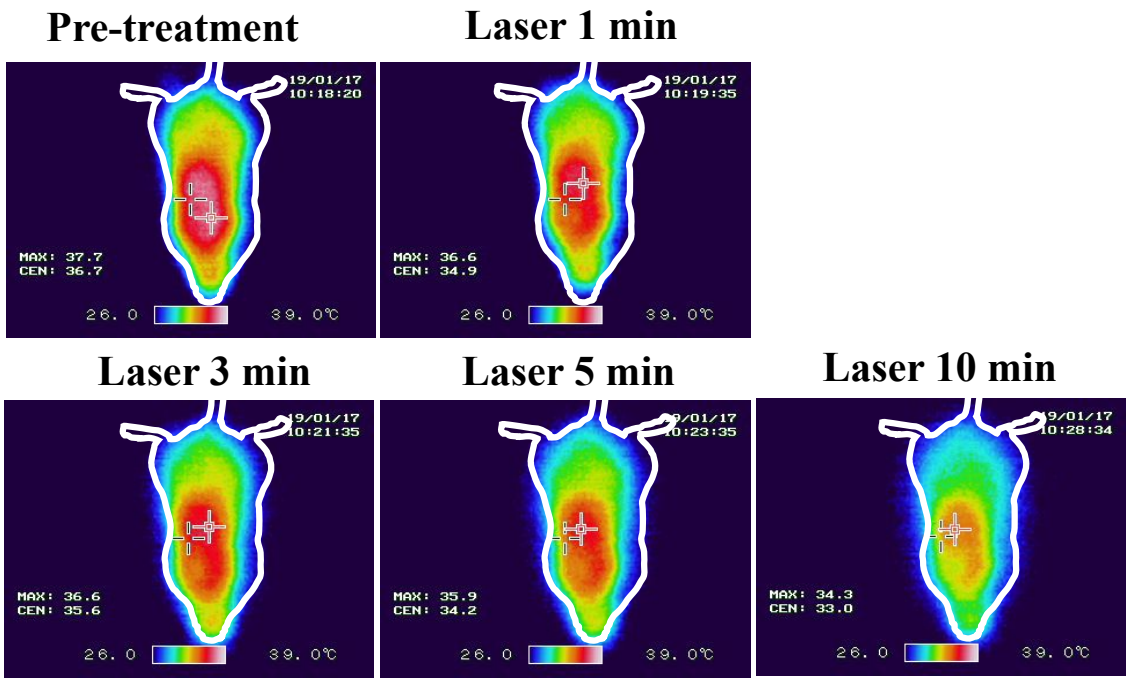

Figure S11. The observation of the NIR-thermal imaging on wound sites following PB colloids + Laser (0.5 W/cm^2) treatment at pre-treatment and laser exposure in the course of 1, 3, 5, and 10 min.

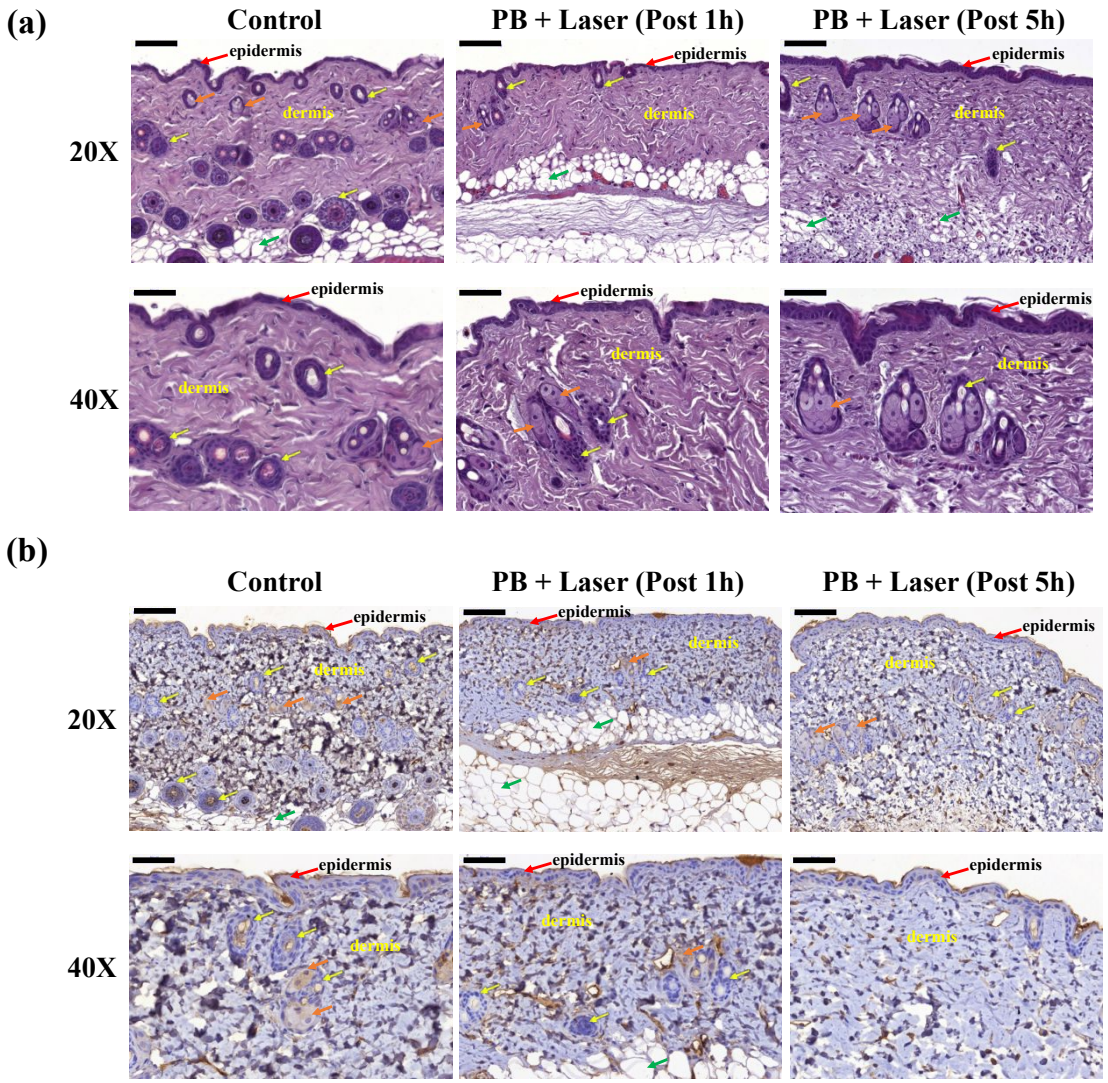

Figure S12. The immunohistochemical staining in (a) hematoxylin and eosin (H&E) and (b) phospho-histone H2A.X for wounds treated with PB colloids (100 ppm) + Laser at different post-periods. (yellow arrow: hair follicle; orange arrow: sebaceous gland; green arrow: adipocytes. Scale bars: 100 μm for 20X; 50 μm for 40X)

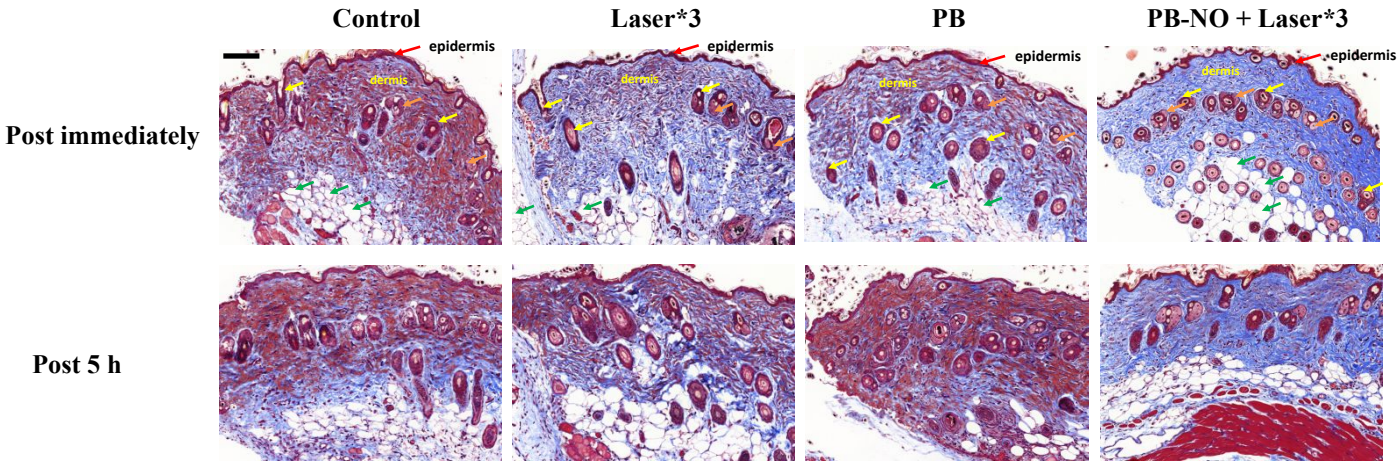

Figure S13. Representative photographs (scale bar = 100 μm) of the immunohistochemical staining in Masson's trichrome for wound regions treated with H_2O (control), H_2O + Laser (Laser*3), PB colloids (100 ppm), and PB-NO colloids (100 ppm) + Laser*3 at post- immediately and -5 h. (yellow arrow: hair follicle; orange arrow: sebaceous gland; green arrow: adipocytes; blue color: collagen; n = 3).

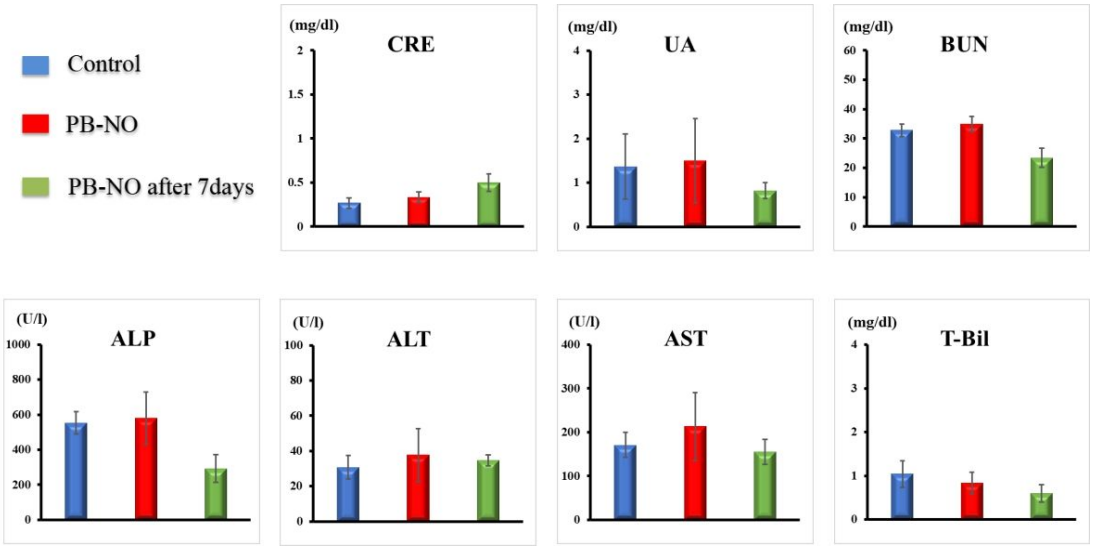

Figure S14. Blood biochemical analysis was used to monitor kidney and liver function indices. The H_2O (as control) and PB-NO colloids (100 ppm in Fe concentration) were directly dropped on the wounds. The blood was collected immediately after treatment (red column) and at post-treatment 7^{th} day (green column). (CRE: creatinine, UA: uric acid, BUN: blood urea nitrogen, ALP: alkaline phosphatase, ALT: alanine transaminase, AST: aspartate transaminase, and T-Bil: total bilirubin, n = 3).

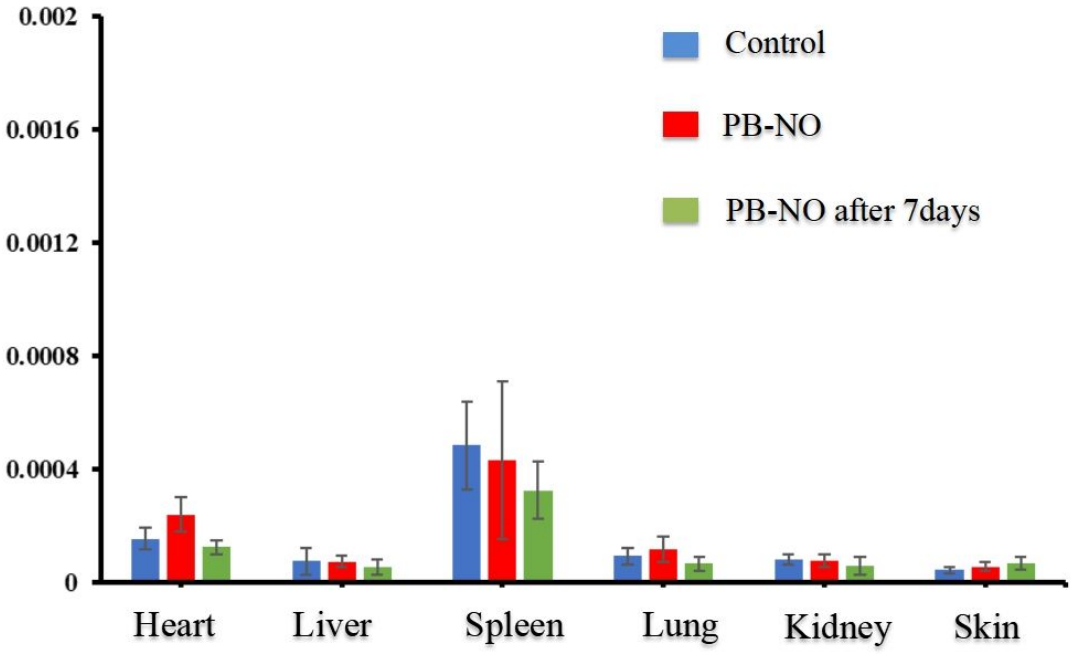

Figure S15. Biodistribution of PB-NO colloids in major organs and the skin around the wounds was tracked based on Fe content. The H_2O (as control) and PB-NO colloids (100 ppm in Fe concentration) were directly dropped on the wounds. The organs and skin were collected immediately after treatment (red column) and at post-treatment 7^{th} day (green column) (n = 3).

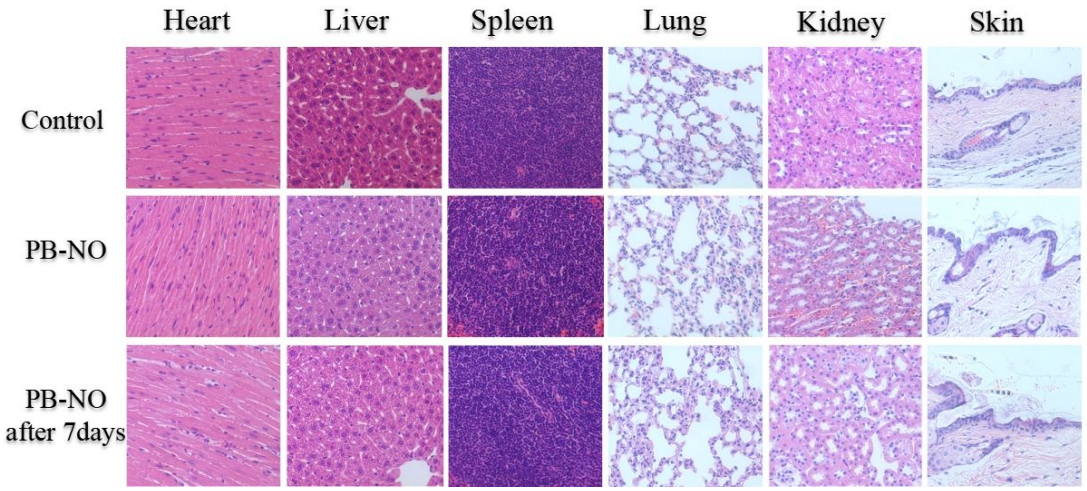

Figure S16. H&E stained tissues were taken from heart, liver, spleen, lung, kidney and skin around the wound. The H_2O (as control) and PB-NO colloids (100 ppm in Fe concentration) were directly dropped on the wounds. The tissues were collected immediately after treatment and at post-treatment 7^{th} day (n = 3).

Calculation of hemin modification efficiency for PB-Hemin nanocubes.

The amount of hemin on single PB-Hemin nanocube were calculated to determine the modification efficiency.

The final concentration of PB-NH_2 nanocubes for hemin modification in our preparation procedure was fixed to be 800 ppm (concentration of iron) in 10 mL reaction solution.

Therefore, we can obtain the total weight of iron in this solution to be 8×10^{-3} g, and the total weight of Prussian blue was determined to be 1.76×10^{-3} g.

The diameter (d) of nanocube is 100 nm, and the volume (V) of nanocube can be calculated by the following equation.

$V = d^3$

Thus, the volume of nanocube is 1×10^{-15} cm^3.

The density (D) of Prussian blue is 1.8 g/cm^3.

Thereby, we can calculate the weight (W) of single nanocube by the equation:

$$D = \frac{W}{V}$$

Accordingly, the weight of single nanocube is 1.8×10^{-15} g.

And then, the total number of nanocubes in hemin modification reaction can be obtained through the total weight of Prussian blue divided by the weight of single nanocube resulting in 1×10^{13}.

Taking the absorbance of hemin at 403 nm, we can estimate the hemin in suspension before and after hemin modification to determinate how many hemin molecules were modified on the nanocubes.

A decrease of absorbance can be observed from UV spectrum of hemin in supernatant after reaction (Figure S17). Therefore, the amount of hemin modified on PB-NH_2 can be calculated through a calibration curve of absorbance *v.s.* concentration of hemin. Thus, the weight of hemin on nanocubes was found as 1.3×10^{-4} g.

The molecular weight of hemin and Avogadaros's number is 652 g/mole and 6×10^{23}, respectively. The total number of hemin on nanocubes can be calculated as 1.2×10^{17}.

Finally, we can calculate the hemin modification efficiency to be 1.2×10^{4} (hemin/ per nanocube).

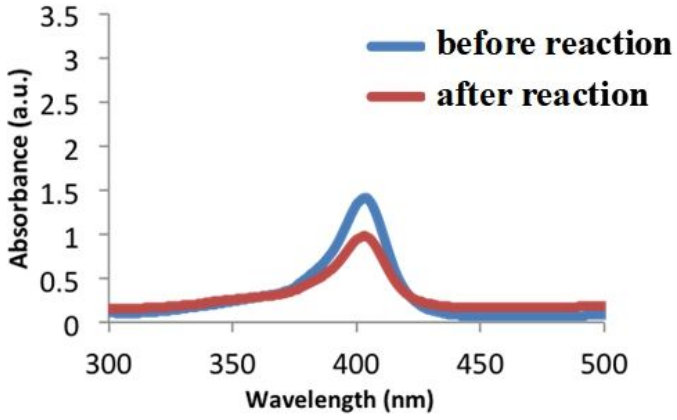

Figure S17. The UV-Vis spectrum of hemin in the suspension before and after modification reaction.